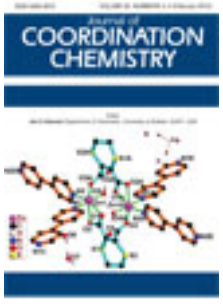


Journal of Coordination Chemistry
Publication details, including instructions for authors and subscription information:
http://www.tandfonline.com/loi/gcoo20

# Properties of 2-, 3-, and 4-acetylpyridine substituted ruthenium(II) bis(bipyridine) complexes: substituent effect on the electronic structure, spectra, and photochemistry of the complex

Amer A.G. Al Abdel Hamid [a] & Sofian Kanan [b]
[a] Department of Chemistry , Yarmouk University , Irbid , Jordan
[b] Department of Biology & Chemistry , American University of Sharjah , United Arab Emirates
Published online: 24 Jan 2012.

To cite this article: Amer A.G. Al Abdel Hamid & Sofian Kanan (2012) Properties of 2-, 3-, and 4-acetylpyridine substituted ruthenium(II) bis(bipyridine) complexes: substituent effect on the electronic structure, spectra, and photochemistry of the complex, Journal of Coordination Chemistry, 65:3, 420-430, DOI: 10.1080/00958972.2011.653350

To link to this article: http://dx.doi.org/10.1080/00958972.2011.653350

*Journal of Coordination Chemistry*
Vol. 65, No. 3, 10 February 2012, 420–430



# Properties of 2-, 3-, and 4-acetylpyridine substituted ruthenium(II) bis(bipyridine) complexes: substituent effect on the electronic structure, spectra, and photochemistry of the complex

AMER A.G. AL ABDEL HAMID*† and SOFIAN KANAN‡

†Department of Chemistry, Yarmouk University, Irbid, Jordan
‡Department of Biology & Chemistry, American University of Sharjah, United Arab Emirates

(*Received 10 August 2011; in final form 11 November 2011*)

Bis(2,2′-bipyridine) complexes of ruthenium(II) with 2-, 3-, and 4-acetylpyridine derivatives were synthesized and structurally characterized. The effect of changing the location of the pyridine's acetyl substituent was studied experimentally and theoretically to clarify the effect of substituent position on the chemical behavior and photochemical properties of the complex. The substituent position on the heterocyclic-pyridine was found to strongly affect the chemical and photochemical properties of the complex. Variation of the position of the substituent, and thus ligand modification brought by as a consequence of this variation, offers possibilities to design complexes of desired structural and photochemical properties.

*Keywords*: Ruthenium(II); 2,2′-Bipyridine; Acetylpyridine; Substituent effect; Position effect



## 1. Introduction

Ruthenium(II) complexes containing N-donor heterocyclic ligands are widely studied [1–5]. The intense absorption in the visible and near-UV region, coupled to catalytic and photo/electrochemical applications, is one among the most important properties that drew interest to this category of complexes [5–10]. The structural properties of the interacted bipyridine ligand, i.e. the existence of substituents and their position on the heterocyclic ring system, strongly affect the photochemistry and catalytic properties of these complexes [11, 12]. Various electrochemical applications of such bipyridine/pyridine-substituted ruthenium systems are based on the relatively low MLCT energy, which mainly involves electron transfer from metal d-orbitals to ligand $\pi^*$-orbitals [12]. Electronic properties of such Ru(II)-bipyridine/pyridine complexes can be effectively manipulated by ligand exchange or modification. It has been reported that variation of the ligand sphere can induce changes in the electron distribution around the metal center and, in turn, modify the photochemical properties of the complexes [13, 14].

*Corresponding author. Email: amerj@yu.edu.jo


ISSN 0095-8972 print/ISSN 1029-0389 online 
http://dx.doi.org/10.1080/00958972.2011.653350

Therefore, the tunability of the photochemical properties by changing the positions of the substituents on the bipyridine/pyridine derivatives can be utilized in designing complexes with desired absorption properties.

To gain deeper understanding of the variations in location of the substituents attached to the heterocyclic ring of bipyridine/pyridine systems and consequently, the effect on the properties of the complexes, a systematic experimental and modeling study has been carried out. Three new acetylpyridine-based ruthenium(II) bis(bipyridine) complexes have been synthesized and characterized. Variations in the position of the acetyl substituent on the pyridine have been made. The dependence of the chemical and photochemical properties of the ruthenium complexes on the ligand substituent location (acetyl group) affects the complex photochemical properties. The computational work aims to reliably predict the stability of the complexes and to use structure simulations to aid in understanding the effect of substituent on ligand design with desired properties.



## 2. Experimental

### 2.1. *General*

All reagents were obtained from commercial sources and used without purification. Column chromatography was performed with silica gel 60 A/35–70 μm, Merck $Al_2O_3$ 90 basic (0.063–0.200 mm). $^1H$ and $^{13}C$ NMR spectra were recorded on a Bruker 400 MHz. The chemical shifts are reported using the residual solvent signal as an indirect reference to TMS: DMSO-$d_6$ 2.05 ppm ($^1H$) and 29.84 ppm ($^{13}C$). UV-Vis spectra were recorded for solutions on a Shimadzu UV-1800 spectrophotometer using 1 cm quartz cuvettes. Infrared (IR) spectra were collected on a JASCO FT/IR-4100 spectrometer. All IR spectra were recorded as pressed KBr discs. Typically, for each spectrum, 100 scans were averaged at 4 $cm^{-1}$ resolution. Microanalyses (C, H, and N) were performed using a Euro EA elemental analyzer 3000. Conductivity measurements were carried out using a JENWAY 4010 conductivity meter employing 0.001 mol $L^{-1}$ solutions of the complex. Thermal measurements (TGA and DTG) were recorded on a NETZSCH model TG-209F1 instrument using 10 mg samples. Magnetic measurements were performed using a Sherwood Scientific instrument.

### 2.2. *Synthesis*

**2.2.1. *Cis*-ruthenium-bis(2,2′-bipyridine)dichloride dihydrate, $Ru(bpy)_2Cl_2 \cdot 2H_2O$.** This was prepared and characterized according to Sullivan *et al*. [15].

**2.2.2. *Cis*-ruthenium-bis(2,2′-bipyridine)-bis(2-acetylpyridine)-bis(hexafluorophosphate), (Ru–Py2K).** $Ru(bpy)_2Cl_2 \cdot 2H_2O$ (200 mg, 0.4 mmol) and 2-acetylpyridine (Py2K), 97 mg, 0.8 mmol) were dissolved separately in 20 mL absolute ethanol. After mixing, the resulting solution was subjected to reflux overnight (24 h) after which $NH_4PF_6$ (2.0 g, 12.5 mmol) dissolved in 5 mL water was added to precipitate the complex. After cooling the reaction mixture for 1 h in an ice bath, the solid product was collected by suction filtration and washed thoroughly with 10 mL portions of water followed by

diethyl ether. The complex was air dried to yield 0.22 g (56%), m.p. 222–224°C (dec.). Found: C, 42.57; H, 3.13; N, 7.92; Calcd for $C_{34}H_{30}F_{12}N_6P_2O_2Ru \cdot 2H_2O$: C, 41.60; H, 3.49; N, 8.56. $^1$H-NMR 400 MHz (DMSO-$d_6$) $\delta$ (ppm) 8.88(d, $J = 8.0$ Hz, 1H, H-6, pyCOCH$_3$), 8.84(d, $J = 7.6$ Hz, 1H, H-6′, pyCOCH$_3$), 8.80(d, $J = 8.0$ Hz, 2H, H-5′,5″, bpy), 8.76(d, $J = 8.0$ Hz, 1H, H-5, bpy), 8.72(d, $J = 8.0$ Hz, 1H, H-5‴, bpy), 8.30(d, $J = 8.0$ Hz, 1H, H-2, bpy), 8.20(d, $J = 8.0$ Hz, 1H, H-2′, bpy), 8.15(d, $J = 8.0$ Hz, 1H, H-2″, bpy), 8.10(d, $J = 6.4$ Hz, 1H, H-2‴, bpy), 8.01(d, $J = 1.3$ Hz, 1H, H-3, pyCOCH$_3$), 7.98(d, $J = 1.3$ Hz, 1H, H-3′, pyCOCH$_3$), 7.90(t, $J = 6.5$ Hz, 2H, H-4,4′, pyCOCH$_3$), 7.85(dd, $J = 8.4$, 2.1 Hz, 2H, H-4,4‴, bpy), 7.77(dd, $J = 8.4$, 2.1 Hz, 2H, H-4′,4″, bpy), 7.71(t, $J = 6.5$ Hz, 2H, H-5,5′, pyCOCH$_3$), 7.65(t, $J = 6.4$ Hz, 1H, H-3, bpy), 7.60(t, $J = 5.4$ Hz, 1H, H-3′, bpy), 7.50(t, $J = 6.0$ Hz, 1H, H-3″, bpy), 7.45(t, $J = 6.0$ Hz, 1H, H-3‴, bpy), 2.08(s, 6H, CH$_3$, pyCOCH$_3$). $^{13}$C NMR (DMSO-$d_6$) $\delta$ (ppm) 214.4(2CO), 158.5(C-2,2′, pyCOCH$_3$), 157.4(C-6,6‴, bpy), 157.2(C-6′,6″, bpy), 156.8(C-2,2‴, bpy), 156.3(C-2′,2″, bpy), 152.9(C-6,6′, pyCOCH$_3$), 152.5(C-4,4‴, bpy), 152.2(C-4′,4″, bpy), 151.8(C-4,4′, pyCOCH$_3$), 138.5(C-5,5′, pyCOCH$_3$), 138.1(C-5,5‴, bpy), 137.9(C-5′,5″, bpy), 132.7(C-3,3‴, bpy), 132.4(C-3′, 3″, bpy), 127.8(C-3, pyCOCH$_3$), 124.2(C-3′, pyCOCH$_3$), 26.4(CH$_3$), 25.6(CH$_3$)′; UV-Vis $\lambda_{max}$ ($\varepsilon$) 293 nm ($7.1 \times 10^4$), 350 nm(sh) ($1.5 \times 10^4$), 475 nm ($1.3 \times 10^4$).

**2.2.3. *Cis*-ruthenium-bis(2,2′-bipyridine)-bis(3-acetylpyridine)-bis(hexafluorophosphate), (Ru–Py3K) and *cis*-ruthenium-bis(2,2′-bipyridine)-bis(4-acetylpyridine)-bis(hexafluorophosphate), (Ru–Py4K).** These were prepared employing the same procedures as mentioned above for Ru–Py2K. Excluding errors in weighing, the exact quantities of the reagents and starting materials ($Ru(bpy)_2Cl_2 \cdot 2H_2O$ and Py3K or Py4K) are used in the reaction mixture as outlined in the preparation of Ru–Py2K. After air drying, the Ru–Py3K complex was 0.31 g (80%), m.p. 210–212°C (dec.). Found: C, 42.78; H, 3.47; N, 8.51; Calcd for $C_{34}H_{30}F_{12}N_6P_2O_2Ru \cdot 2H_2O$: C, 41.60; H, 3.49; N, 8.56. $^1$H-NMR 400 MHz (DMSO-$d_6$) $\delta$ (ppm) 9.07(s, 1H, H-6, pyCOCH$_3$), 9.04(s, 1H, H-6′, pyCOCH$_3$)′), 8.70(t, $J = 8.2$ Hz, 4H, H-4,4′,4″,4‴, bpy), 8.52(t, $J = 7.1$ Hz, 4H, H-3,3′,3″,3‴, bpy), 8.42(d, $J = 5.9$ Hz, 2H, H-2,2′, pyCOCH$_3$), 8.26(t, $J = 8.2$ Hz, 2H, H-3,3′, pyCOCH$_3$), 8.05(dd, $J = 5.8$, 5.9 Hz, 4H, H-5,5′,5″,5‴, bpy), 7.88(t, $J = 8.2$ Hz, 2H, H-4,4′, pyCOCH$_3$), 7.55(dd, $J = 4.7$, 5.9 Hz, 4H, H-2,2′,2″,2‴, bpy), 2.51(s, 3H, CH$_3$, pyCOCH$_3$), 2.45(s, 3H, ′CH$_3$, (pyCOCH$_3$)′). $^{13}$C NMR (DMSO-$d_6$) $\delta$ (ppm) 195.7(2CO), 157.1(C-2,2‴, bpy), 156.8(C-2′,2″, bpy), 156.6(C-2, 2′, pyCOCH$_3$), 152.3(C-6,6′,6″,6‴, bpy), 152.2(C-6, C-6′, pyCOCH$_3$), 138.2(C-4′, 4″, bpy), 138.0(C-4,4‴, bpy), 137.4(C-4,4′, pyCOCH$_3$), 133.9(C-3,3′, pyCOCH$_3$), 128.2(C-5, C-5‴, bpy), 127.9(C-5,5″, bpy), 126.3(C-5,5′, pyCOCH$_3$), 124.2(C-3′, C-3″, bpy), 123.9(C-3,3‴, bpy), 26.9(2CH$_3$); UV-Vis $\lambda_{max}$ ($\varepsilon$) 293 nm ($5.1 \times 10^4$), 350 nm ($1.1 \times 10^4$), 440 nm ($7.9 \times 10^3$).

The air dried complex Ru–Py4K was 0.24 g (62 %), m.p. 243–246°C (dec.). Found: C, 43.49; H, 3.24; N, 8.74; Calcd for $C_{34}H_{30}F_{12}N_6P_2O_2Ru \cdot H_2O$: C, 42.38; H, 3.35; N, 8.72. $^1$H-NMR 400 MHz (DMSO-$d_6$) $\delta$ (ppm) 9.85(d, $J = 6.6$ Hz, 2H, H-6,6′, pyCOCH$_3$), 8.82(d, $J = 5.1$ Hz, 2H, H-2,2′, pyCOCH$_3$), 8.70(d, $J = 7.3$ Hz, 4H, H-5,5′,5″,5‴, bpy), 8.60(d, $J = 8.2$ Hz, 2H, H-2,2′, bpy), 8.50(d, $J = 5.3$ Hz, 2H, H-6,6′, bpy), 8.20(dd, $J = 7.2$, 6.7 Hz, 1H, H-4′, bpy), 7.90(dd, $J = 8.2$, 7.1 Hz, 1H, H-4″, bpy), 7.83(d, $J = 5.2$ Hz, 2H, H-5,5′, pyCOCH$_3$), 7.73(t, $J = 4.2$ Hz, 2H, H-4,4‴, bpy), 7.57(d, $J = 5.7$ Hz, 2H, H-3,3′, pyCOCH$_3$), 7.37(t, $J = 6.8$ Hz, 2H, H-3,3‴, bpy),

Table 1. Analytical and physical data of the ruthenium complexes with isomeric forms of acetylpyridine.

| Compound | % C Exp. (Calcd) | % H Exp. (Calcd) | % N Exp. (Calcd) | Color/look | $\Lambda^a$ ($\Omega^{-1}\,cm^2\,mol^{-1}$) |
|---|---|---|---|---|---|
| Ru–Py2K · $2H_2O$ | 42.57 (41.60) | 3.13 (3.49) | 7.92 (8.56) | Purple/powder | 265 |
| Ru–Py3K · $2H_2O$ | 42.78 (41.60) | 3.47 (3.49) | 8.51 (8.56) | Red/crystalline powder | 278 |
| Ru–Py4K · $H_2O$ | 43.49 (42.38) | 3.24 (3.35) | 8.74 (8.72) | Yellow/powder | 273 |

[a]DMSO solutions, 0.001 mol $L^{-1}$ at 25°C.



7.30(t, $J = 6.8$ Hz, 2H, H-3,3″, bpy), 2.98(s, 3H, $CH_3$, py$COCH_3$), 2.55(s, 3H, $'CH_3$, (py$COCH_3$)′). $^{13}$C NMR (DMSO-$d_6$) $\delta$ (ppm) 196.9(2CO), 158.7(C-6′, bpy), 157.8(C-6, bpy), 157.5(C-6″, bpy), 157.2(C-6‴, bpy), 154.3(C-2,2′, py$COCH_3$), 152.5(C-2‴, bpy), 152.3(C-2, bpy), 151.7(C-2′, bpy), 151.4(C-2″, bpy), 141.9(C-6,6′, py$COCH_3$), 136.8(C-4,4′, py$COCH_3$), 136.4(C-4,4″, bpy), 136.3(C-4′, bpy), 135.7(C-4‴, bpy), 127.3(C-3,3′, py$COCH_3$), 127.2(C-5′, bpy), 126.7(C-5, bpy), 126.2(C-5,5′, py$COCH_3$), 123.9(C-5‴, bpy), 123.6(C-5″, bpy), 123.5(C-3′, bpy), 123.2(C-3″,3‴, bpy), 122.4(C-3, bpy), 26.8($2CH_3$); UV-Vis $\lambda_{max}$ ($\varepsilon$) 293 nm ($7.1 \times 10^4$), 360 nm ($1.1 \times 10^4$), 408 nm ($1.2 \times 10^4$), 491 nm ($1.8 \times 10^4$).

### 2.3. *Theoretical computations*

Geometry optimizations of the non-bonded (free) ligands were performed by the *ab initio* RHF method using the LANL2DZ basis set [2, 16–18]. LANL2DZ effective core potential basis set was employed to study both the ligands and the oversimplified simulated structures of ruthenium complexes in the same theoretical framework. The primary goal of these calculations was to obtain the vibrational frequency of the carbonyl group of the free and coordinated acetylpyridines. The second goal was to calculate (and thus compare) the minimum energy of complexes when coordination to metal ion takes place *via* nitrogen compared to oxygen. All systems have been optimized without symmetry restrictions or solvent effect consideration. All calculations were performed with Gaussian 03 package [19].

## 3. Results and discussion

### 3.1. *Synthesis*

Ru–Py2K, Ru–Py3K, and Ru–Py4K were isolated as dark brown, orange-reddish, and brown solid powders, respectively (table 1). Their yields are relatively high (74–89%) by the reaction of the ruthenium-bipyridine complex, $Ru(bpy)_2Cl_2 \cdot 2H_2O$, with 2-, 3-, and 4-acetylpyridine in 1 : 2 (metal : ligand) mole ratio in absolute ethanol using a single step procedure. The representative structure of the three complexes is presented in figure 1. The formed complexes were observed precipitate in the reaction vessel upon cooling and after addition of the precipitating agent, ammonium hexafluorophosphate. In DMSO, Ru–Py2K, Ru–Py3K, and Ru–Py4K gave rise to four absorptions, two strong bands in the UV region at 293 and 350 nm, and two medium intensity broad

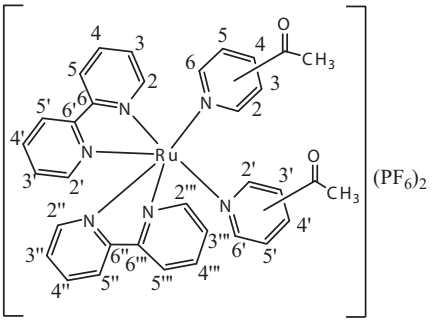


Figure 1. Simplified structure of the *cis*-ruthenium-bis(2,2′-bipyridine)-bis(2-, 3-, or 4-acetylpyridine)-bis(hexafluorophosphate), (Ru–Py2K(ortho-acetyl group), Ru–Py3K(meta-acetyl group), and Ru–Py4K (para-acetyl group)).

Table 2. UV-Vis spectral data in DMSO.

| Compound | $\lambda_{max/nm}$ (log $\varepsilon$) | Stretching frequency of CO ($cm^{-1}$) |
|---|---|---|
| $Ru(bpy)_2Cl_2 \cdot 2H_2O$ | 256 (4.32)<br>295 (4.60)<br>376 (3.95), broad<br>556 (3.97), broad | – |
| Py2K | 326 (1.80) | 1702 [21] |
| Py3K | 329 (1.80), broad | 1690 [20] |
| Py4K | No bands | 1697 [20] |
| Ru–Py2K | 293 (4.85)<br>350 (4.17)<br>450 (4.11), broad<br>506 (4.10), broad | 1698 |
| Ru–Py3K | 293 (4.71)<br>350 (4.04)<br>426 (3.90), broad<br>457 (3.88), broad | 1698 |
| Ru–Py4K | 293 (4.85)<br>350 (4.04)<br>408 (4.08), broad<br>493 (4.26), broad | 1698 |

bands in the visible region. In Ru–Py2K, the two visible bands were at 450 and 506 nm, while in Ru–Py3K, 426 and 457 nm and at 408 and 493 nm for Ru–Py4K. The structures of the Ru–Py2K, Ru–Py3K and Ru–Py4K, figure 1, were verified by IR, $^1$H- and $^{13}$C-NMR, elemental analysis, magnetic susceptibility, and conductivity measurements.

Introduction of acetylpyridine into $Ru(bpy)_2Cl_2 \cdot 2H_2O$ is evidenced by the appearance of the characteristic ketonic carbonyl IR-band at 1698 $cm^{-1}$, table 2. Appearance of this band at this specific frequency [20], which is very close to that [20, 21] in free acetylpyridines (1690–1702 $cm^{-1}$, table 3), clearly indicates that acetylpyridine derivatives coordinate through nitrogen of the pyridine ring [20] and not through oxygen of carbonyl. In support of this interpretation, *ab initio* calculations using model

Table 3. Calculated minimum energy of the Ru–N and Ru–O bound simulated complexes.

| Compound | Energy (Hartrees) | $\Delta E = E_N - E_O$* (kcal mol$^{-1}$) |
|---|---|---|
| Ru–Py2K (Ru···N) | −491.279 | −45.808 |
| Ru–Py2K (Ru···O) | −491.206 | |
| Ru–Py3K (Ru···N) | −491.315 | −7.530 |
| Ru–Py3K (Ru···O) | −491.303 | |
| Ru–Py4K (Ru···N) | −491.326 | −130.522 |
| Ru–Py4K (Ru···O) | −491.118 | |

*$\Delta E = E_N - E_O$ is calculated by finding the energy difference (in kcal mol$^{-1}$) between the minimum energies of the N–Ru bound complex and the corresponding O–Ru bound complex.



compounds of ruthenium (and some other ions) that interacted with the three isomeric forms of acetylpyridine were performed. In all cases, the computations indicated that coordination of the Ru to nitrogen of acetylpyridine produced a more stable complex than Ru coordinated to oxygen of carbonyl. No change was found in the calculated stretching frequency of the carbonyl group when ruthenium was bound to the pyridine nitrogen. These computational findings enforce the experimental conclusion about coordination of ruthenium through pyridine. Very few sources [7, 22] have reported that acetylpyridines are bidentate through N of pyridine and O of CO, simultaneously.

The strong band at 842 cm$^{-1}$ in spectra of the complexes with acetylpyridine (Supplementary material), and not in spectrum of the starting complex $Ru(bpy)_2Cl_2 \cdot 2H_2O$ (Supplementary material), can safely be ascribed [23] to $PF_6^-$ ($\nu_{P-F} = 842\,cm^{-1}$). The broad band at 1573 cm$^{-1}$ in spectra of the three complexes corresponds to the overlapped stretching vibrations of the pyridine (C=N and C=C) [7, 22, 24]. This band is shifted to lower frequency compared to that [7, 9, 22, 24, 25] in free pyridines (1585 cm$^{-1}$). The same band is at 1610 cm$^{-1}$ in $Ru(bpy)_2Cl_2 \cdot 2H_2O$. The lower energy observed for this band (at 1573 cm$^{-1)}$ compared to free pyridines arises from $\pi$-back donation from ruthenium [20] to the anti-bonding orbitals of the ligands. In contrast, the C=N and C=C bonds in $Ru(bpy)_2Cl_2 \cdot 2H_2O$ have more double bond character due to the withdrawal effect of electrons by the adjacent chlorides, prohibiting $\pi$-back donation to the ligand, thus causing a blue shift in the band (1610 cm$^{-1}$ compared to that in free pyridines). The medium intensity band at 557 cm$^{-1}$, which appears in spectra of the complexes and not in $Ru(bpy)_2Cl_2 \cdot 2H_2O$, is assigned to the stretching vibration of Ru–N(acetylpyridine) in the *cis*-configuration [26]. The band at 763 cm$^{-1}$ is assigned to C–H bend of the pyridine ring [20, 26].

$^1$H- and $^{13}$C-NMR, in terms of the peak shift and number of peaks along with the conductivity measurements and elemental analysis results for C, H, and N, are consistent with the general structure proposed in figure 1.

### 3.2. *Electronic spectra*

Table 2 lists the electronic absorption bands for DMSO solutions of Ru–Py2K, Ru–Py3K, and Ru–Py4K, along with the absorption bands of Py2K, Py3K, and Py4K. The UV-bands in the Ru–Py2K, Ru–Py3K, and Ru–Py4K complexes are assigned to the internal bipyridine ligand electronic transitions. These bands are very close in energy and intensity to those encountered in $Ru(bpy)_2Cl_2 \cdot 2H_2O$ [15] which only contains bipyridine. In similar complexes (where ruthenium is only coordinated to

2,2′-bipyridine) identical absorptions have been reported [15, 26]. These absorptions are attributed to the bipyridine localized $\pi \rightarrow \pi^*$ intraligand transition. This transition is known to occur at 280 nm in free 2,2′-bipyridine and when coordinated to ruthenium a bathochromic shift was observed in the transition [15, 26].

In addition to UV-bands, each complex exhibits two additional bands in the visible region. Based on their molar absorptivities (which range from 8 to $20 \times 10^3\,\mathrm{mol^{-1}\,cm^{-1}\,L}$), these bands are assigned to MLCT from filled $d\pi$-$Ru^{II}$ orbitals to the multiple low-lying $\pi^*$ orbitals of the ligands. This kind of MLCT transition is expected to produce an excited state that is mainly singlet (e.g., $d\pi^6 \rightarrow d\pi^5\pi^{*1}$) but possesses significant triplet character due to spin–orbit coupling. In the order Ru–Py2K, Ru–Py4K to Ru–Py3K, the lowest energy visible band decreases ($506 > 493 > 457$ nm) in wavelength, in parallel with the increased acidity of the ligand as a result of the inductive effect induced on the N-donor by the adjacent acetyl substituent which is electron withdrawing.

The visible bands at 506–457 nm are attributed to the MLCT transition from the $d\pi$-$Ru^{II}$ metal-like molecular orbital to a ligand-like molecular orbital with a larger contribution from the pyridine nitrogen. Visible bands at 450–408 nm are associated with a similar MLCT transition but with a larger contribution from the pyridine oxygen. Haukka *et al.*, in a computational study [12], concluded that molecules with alkoxy carbonyl-substituents at the *para*- and *meta*-positions of the bipyridine ring have much lower energy compared to compounds with substituents at the *ortho*-positions. Based on their conclusion, the geometric strain was responsible for this increase in energy. Furthermore, they related the photochemical properties of the metal complexes to the energy differences between the highest occupied (HOMO) and the lowest unoccupied (LUMO) molecular orbitals. The energy difference between HOMO and LUMO was shown to be adjustable by the electronic character and position of the substituent. Complexes in which alkoxy carbonyl (as electron withdrawing group) was positioned at the *para*-position have shown a narrower HOMO–LUMO energy gap than the unsubstituted complexes, while substitution at *ortho*- and *meta*-positions led to larger energy differences. Our experimental findings agree with the conclusions of Haukka in the dependence of the photochemical properties of complexes on substituent location (with respect to the N-donor atom) on pyridine. Correlating the computed minimum energies of the three complexes with the wavelengths of their visible bands clearly shows that *ortho*-substituted Ru–Py2K has the longest wavelengths compared to Ru–Py3K (*meta*-substituted) and Ru–Py4K (*para*-substituted). The transition from HOMO to LUMO requires the least energy (narrowest HOMO–LUMO gap) compared to the corresponding transitions in Ru–Py3K and Ru–Py4K. In other words, the effect of the substituent at the *ortho*-position has the greatest effect on stability and thus photochemical properties of the complex compared to the substituents at the *meta* and *para* positions. The *para*-substituted Ru–Py4K showed the greatest stability (least computed minimum energy, table 3) and as a result, the electronic transitions require high energy to cross the wide HOMO–LUMO gap, so the wavelengths of the transitions came closer to the UV than to the visible region.

### 3.3. *Molar conductance*

The molar conductivity values of the complexes, Ru–Py2K, Ru–Py3K, and Ru–Py4K, are determined to be in the order 265, 278, and $273\,\Omega^{-1}\,\mathrm{cm^2\,mol^{-1}}$, respectively.

These values suggest the existence of the complexes as 1 : 2 species compared to other known Ru(II) complexes [27].

### 3.4. *Magnetic susceptibility*

The negative magnetic susceptibility values obtained for all of the complexes reveal that ruthenium exists as $d^6$-low spin Ru(II) with no unpaired electrons. This is a very common spin state for ruthenium metal ions when coordinated to strong field ligands like pyridine derivatives [25].



### 3.5. *Thermal analyses*

Thermal analysis (TGA and DTGA) curves of the three complexes were carried out within a temperature range of 25–1000°C; the curve for the Ru–Py3K is shown in "Supplementary material" as an example. The estimated mass losses were determined based on the TGA/DTGA-thermograms and the calculated mass losses were computed. Percent mass losses and temperature range of each stage are included in table 4. In addition, the table includes the thermal effect(s) accompanying the change in solid complex on heating for every stage. The three complexes, Ru–Py2K, Ru–Py3K, and Ru–Py4K, each give five stages of decomposition. The first step in each complex at 25–270°C represents the loss of water(s) of hydration. Ru–Py2K and Ru–Py4K together showed identical thermograms compared to Ru–Py3K. The close similarity in the thermal effects among the five stages of the two complexes is clear (table 4). For example, both complexes lost the two acetylpyridine ligands at once and ended up with the same residues, $Ru(bpy)_2$. However, the two complexes are dissimilar in terms of the temperature ranges at which various thermal effects took place. Obviously, in Ru–Py2K, loss of the fragments occurred at lower temperatures compared to their analogs in the Ru–Py4K complex. For example, Ru–Py2K lost the two acetylpyridines at 340–537°C, whereas Ru–Py4K lost the same fragments at 390–565°C. Similarly,

Table 4. Thermoanalytical (TG) results of the ruthenium complexes with isomeric forms of acetylpyridine.

| Complex | Temperature range (°C) | Mass loss Estimated (Calcd%) | Thermal effect |
|---|---|---|---|
| Ru–Py2K | 84–214 | 4.12 (3.66) | Loss of the $2H_2O$ hydrate |
| | 260–340 | 15.60 (14.77) | Loss of $PF_6$ |
| | 340–537 | 25.42 (24.68) | Loss of $(PyCOCH_3)_2$ |
| | 567–810 | 14.09 (14.77) | Loss of $PF_6$ |
| | >810 | 41.47 (42.11) | Residue of $Ru(bpy)_2$ |
| Ru–Py3K | 94–220 | 3.54 (3.66) | Loss of $2H_2O$ hydrate |
| | 268–395 | 20.05 (19.14) | Loss of $PF_6$ and $CH_3CO$ |
| | 420–540 | 18.97 (19.14) | Loss of $PF_6$ and $CH_3CO$ |
| | 578–810 | 14.78 (16.12) | Loss of 2py |
| | >810 | 41.37 (42.11) | Residue of $Ru(bpy)_2$ |
| Ru–Py4K | 95–245 | 1.76 (1.87) | Loss of $H_2O$ hydrate |
| | 268–390 | 13.96 (15.04) | Loss of $PF_6$ |
| | 390–565 | 24.70 (25.14) | Loss of $(PyCOCH_3)_2$ |
| | 575–830 | 14.33 (15.04) | Loss of $PF_6$ |
| | >850 | 42.14 (42.91) | Residue of $Ru(bpy)_2$ |

the residue, $Ru(bpy)_2$ in Ru–Py2K, is stable to more than 810°C, while in Ru–Py4K, $Ru(bpy)_2$ was stable until 850°C.

Ru–Py3K shows quite different thermal decomposition behavior compared to Ru–Py2K and Ru–Py4K. Thermal analyses curves (TGA and DTGA) of Ru–Py3K show that it decomposes in five steps. The first at 94–220°C corresponds to loss of water. The second step at 268–395°C corresponds to loss of $PF_6$ and $CH_3CO$ fragments. The estimated mass loss of this step is 20.05%, close to the theoretically calculated 19.14%. The third stage of decomposition at 420–540°C represents loss of the second $PF_6$ and $CH_3CO$ molecules. The estimated mass loss is 18.97% (theoretical 19.14%). The two pyridine rings of the acetyl pyridines are lost in the fourth step. The pattern of losing acetyl pyridines in Ru–Py3K in two steps compared to Ru–Py2K and Ru–Py4K (in which the acetyl pyridines were lost at once) is clearly different. This implies that Ru–N connections in Ru–Py3K (compared to Ru–Py2K and Ru–Py4K) are tightly held and thus require higher temperatures to be detached. From another perspective, this indicates that Ru–N bonding in Ru–Py3K is stronger than Ru–N bonding in Ru–Py2K and Ru–Py4K. The three complexes leave the same chemical moiety as residues.



## 4. Conclusions

The effect of changing the position of the acetyl substituent on the chemical and physical characteristics of ruthenium-bis(2,2′-bipyridine) complexes using 2-, 3-, and 4-acetylpyridines was studied experimentally and computationally. The energy of transitions (HOMO–LUMO gap) and thus the photochemical behavior of the ruthenium complexes were found to depend on the substitution position on the pyridyl ring. Ru–Py2K and Ru–Py4K, by having the acetyl group at *ortho*- and *para*-positions, respectively, behave identically, but different from that observed for Ru–Py3K (in which the acetyl group is *meta*-positioned).

The substitution position affects complex stability and thus its photochemical properties through the electronic inductive effect and the steric effect. In the case of *ortho*-substituted Ru–Py2K, the steric effect is predominant in raising the energy of the complex and thus lowering its stability. However, in *para*-substituted Ru–Py4K, both factors have little effect as a result of the substituent existing away from the N-donor. In *meta*-substituted Ru–Py3K, both effects seem to be counter balanced and, therefore have moderate effect on the stability of the complex. Collectively, the two factors put the stability in the order Ru–Py4K > Ru–Py3K > Ru–Py2K.

Experimentally, the effect of the substituent location on the photochemical properties of the complexes is clear. Considering the wavelength values of the visible bands for instance, we see that Ru–Py3K occupies an intermediate place between the other two extremes, namely the least stable Ru–Py2K and the most stable Ru–Py4K. Ru–Py3K is considered more appropriate to be adopted in colorimetric applications. The high stability of the Ru–Py4K complex (which seems to be attractive at first glance) would leave us with high energy transitions and so produce bands closer to the UV than the visible region.

Variation in the position of the acetyl substituent on the pyridyl ring has a pronounced effect on the ruthenium complex. This variation and the consequent dependence of the photochemical properties of the resulting coordination compound

offer a controlled way to modify the properties of the complex. Changing the position of the substituent on a suitable ligand provides a powerful tool for complex design with certain favorable photochemical properties. The modifiability can be exploited in designing ruthenium bipyridine complexes-based photo-sensitizers in which applications of the substituents on the ligand play a significant role.

## Acknowledgments

This work was supported by Yarmouk University, Faculty of Graduate Studies and Scientific Research. We acknowledge the support by the Department of Chemistry at Jordan University of Science and Technology (JUST) in providing necessary equipment to complete this work. We also thank the Emirates Foundation Group for supporting this work at the American University of Sharjah.



## References

[1] P. Haquette, B. Dumat, B. Talbi, S. Arbabi, J.-L. Renaud, G. Jaouen, M. Salmain. *J. Organomet. Chem.*, **694**, 937 (2009).
[2] I. Calandreli, F. de Souza Oliveira, G. Liang, Z. Novais da Rocha, E. Tfouni. *Inorg. Chem. Commun.*, **12**, 591 (2009).
[3] Y. Chen, W. Liu, B. Liu, X.-H. Zhou, Z.-G. Zou, J.-L. Zuo, X.-Z. You. *Inorg. Chim. Acta*, **362**, 143 (2009).
[4] M. Aydemir, A. Baysal, N. Meric, B. Gümgüm. *J. Organomet. Chem.*, **694**, 2488 (2009).
[5] S. Grgurić-Šipka, I. Ivanović, G. Rakić, N. Todorović, N. Gligorijević, S. Radulović, V.B. Arion, B.K. Keppler, Ž.Lj. Tešić. *Eur. J. Med. Chem.*, **45**, 1051 (2010).
[6] C. Sahin, Th. Dittrich, C. Varlikli, S. Icli, M.Ch. Lux-Steiner. *Sol. Energy Mater. Sol. Cells*, **94**, 686 (2010).
[7] M. Tătucu, P. Rotaru, I. Rău, C. Spînu, A. Kriza. *J. Therm. Anal. Calorim.*, **100**, 1107 (2010).
[8] G. Sathyaraj, T. Weyhermuller, B.U. Nair. *J. Chem. Crystallogr.*, **41**, 353 (2011).
[9] A.E. Graminha, A.A. Batista, J. Ellena, E.E. Castellano, L.R. Teixeira, I.C. Mendes, H. Beraldo. *J. Mol. Struct.*, **875**, 219 (2008).
[10] S. Han, W. Niu, H. Li, L. Hu, Y. Yuan, G. Xu. *Talanta*, **81**, 44 (2010).
[11] O.V. Sizova, N.V. Ivanova, V.V. Sizov, A. Yu Ershov, V.I. Baranovski. *Inorg. Chim. Acta*, **357**, 354 (2004).
[12] T.-J.J. Kinnunen, M. Haukka, T.A. Pakkanen. *J. Organomet. Chem.*, **654**, 8 (2002).
[13] K. Kalyanasundaram, M. Grätzel (Eds). *Photosensitization and Photocatalysis Using Inorganic and Organometallic Compounds*, Kluwer Academic Publishers, Dordrecht (1993).
[14] T.-J.J. Kinnunen, M. Haukka, M. Nousiainen, A. Patrikka, T.A. Pakkanen. *J. Chem. Soc., Dalton Trans.*, 2649 (2001).
[15] B. Sullivan, D.J. Salmon, T.J. Meyer. *Inorg. Chem.*, **17**, 3334 (1978).
[16] (a) T.H. Dunning Jr, P.J. Hay. In *Modern Theoretical Chemistry*, H.F. Schaefer (Ed.), Vol. 3, pp. 79–126, Plenum, New York (1977); (b) T.H. Dunning Jr, *J. Chem. Phys.*, **66**, 1382 (1977), doi: 10.1063/1.434039.
[17] P.J. Hay, W.R. Wadt. *J. Chem. Phys.*, **82**, 270 (1985).
[18] M. Al-Noaimi, M. El-khateeb, S.F. Haddad, M. Sunjuk, R.J. Crutchley. *Polyhedron*, **27**, 3239 (2008).
[19] M.J. Frisch, G.W. Trucks, H.B. Schlegel, G.E. Scuseria, M.A. Robb, J.R. Cheeseman, V.G. Zakrzewski, J.A. Montgomery Jr, R.E. Stratmann, J.C. Burant, S. Dapprich, J.M. Millam, A.D. Daniels, K.N. Kudin, M.C. Strain, O. Farkas, J. Tomasi, V. Barone, M. Cossi, R. Cammi, B. Mennucci, C. Pomelli, C. Adamo, S. Clifford, J. Ochterski, G.A. Petersson, P.Y. Ayala, Q. Cui, K. Morokuma, D.K. Malick, A.D. Rabuck, K. Raghavachari, J.B. Foresman, J. Cioslowski, J.V. Ortiz, A.G. Baboul, B.B. Stefanov, G. Liu, A. Liashenko, P. Piskorz, I. Komaromi, R. Gomperts, R.L. Martin, D.J. Fox, T. Keith, M.A. Al-Laham, C.Y. Peng, A. Nanayakkara, C. Gonzalez, M. Challacombe, P.M.W. Gill, B.G. Johnson, W. Chen, M.W. Wong, J.L. Andres, M. Head-Gordon, E.S. Replogle, J.A. Pople. *Gaussian 98 (Revision A.1)*, Gaussian, Inc., Pittsburgh, PA (1998).

[20] G.M. Rakić, S. Grgurić-Šipka, G.N. Kaluđerović, S. Gómez-Ruiz, S.K. Bjelogrlić, S.S. Radulović, Ž.Ž. Lj. Tešić, *Eur. J. Med. Chem.*, **44**, 1921 (2009).
[21] Y. Kidani, M. Noji, H. Koike. *Bull. Chem. Soc. Japan*, **48**, 239 (1975).
[22] M. Tatucu, A. Kriza, C. Maxim, N. Stanica. *J. Coord. Chem.*, **62**, 1067 (2009).
[23] J. Araujo, S. Nikolaou, A.D.P. Alexiou, H.E. Toma. *Monatsh. Chem.*, **128**, 759 (1997).
[24] K. Nakamoto. *Infrared Spectra of Inorganic and Coordination Compounds*, Wiley, New York (1970).
[25] N.M. Hosny, A.-H.M. Shallaby. *Transition Met. Chem.*, **32**, 1085 (2007).
[26] C.-Y. Duan, Z.-L. Lu, X.-Z. You, T.C.W. Mak. *J. Coord. Chem.*, **46**, 301 (1999).
[27] A.S.A.T. de Paula, B.E. Mann, E. Tfouni. *Polyhedron*, **18**, 2017 (1999).